Journal of
Micro/Nanolithography,
MEMS, and MOEMS

SPIEDigitalLibrary.org/jm3

Defect reduction of high-density full-field patterns in jet and flash imprint lithography

Lovejeet Singh
Kang Luo
Zhengmao Ye
Frank Xu
Gaddi Haase
David Curran
Dwayne LaBrake
Douglas Resnick
S.V. Sreenivasan

SPIE

Defect reduction of high-density full-field patterns in jet and flash imprint lithography

Lovejeet Singh
Kang Luo
Zhengmao Ye
Frank Xu
Gaddi Haase
David Curran
Dwayne LaBrake
Douglas Resnick
S.V. Sreenivasan
Molecular Imprints Inc.
1807-C W. Braker Lane
Austin, Texas 78758
E-mail: Dresnick@militho.com

Abstract. Acceptance of imprint lithography for manufacturing will require demonstration that it can attain defect levels commensurate with the defect specifications of high-end memory devices. We summarize the results of defect inspections focusing on two key defect types: random nonfill defects occurring during the resist filling process and repeater defects caused by interactions with particles on the substrate. Nonfill defectivity must always be considered within the context of process throughput. The key limiting throughput step in an imprint process is resist filling time. Repeater defects typically have two main sources: mask defects and particle-related defects. Previous studies have indicated that soft particles tend to cause nonrepeating defects. Hard particles, on the other hand, can cause either resist plugging or mask damage. We use an Imprio 500 20–wafer per hour development tool to study both defect types. By carefully controlling the volume of inkjetted resist, optimizing the drop pattern, and controlling the resist fluid front during spreading, fill times of 1.5 s are achieved with nonfill defect levels of $\sim$1.2/cm^2. Longevity runs were used to study repeater defects, and a nickel contamination was identified as the key source of particle-induced repeater defects. [DOI: 10.1117/1.3625635]

Subject terms: jet and flash imprint lithography; J-FIL; imprint lithography; imprint masks; templates; defectivity; nonfill defects; repeater defects.

Paper 11070PR received May 11, 2011; revised manuscript received Jul. 19, 2011; accepted for publication Jul. 27, 2011; published online Sep. 14, 2011.

1 Introduction

Imprint lithography has been shown to be an effective technique for replication of nanoscale features.[1,2] Jet and flash imprint lithography (J-FIL^{TM}) involves the field-by-field deposition and exposure of a low-viscosity resist deposited by jetting technology onto the substrate.[3–8] The patterned mask is lowered into the fluid, which then quickly flows into the relief patterns in the mask by capillary action. Following this filling step, the resist is cross-linked under UV radiation and then the mask is removed, leaving a patterned resist on the substrate.

Acceptance of imprint lithography for manufacturing will require demonstration that it can attain defect levels commensurate with the defect specifications of high-end memory devices. Typical defectivity targets are on the order of 0.10/cm^2. Recent studies have marked excellent progress in reducing defects on the mask blank, patterned mask, and imprinted wafer. The master mask blank, which consists of a thin (<10-nm) layer of chromium on the 6 × 6 × 0.25 in. fused silica was recently reported to have a defectivity of only 0.04/cm^2 as measured by a Lasertec tool with 50-nm sensitivity.[9] The improvement in defectivity was driven by the introduction of a supply of low-defect mask blanks and production-quality coat and develop processes. Examples of defectivity on the mask blank, after resist coating and after resist develop are shown in Fig. 1.

Patterned mask defectivity was reported to be $\sim$10/cm^2 as measured by an Hermes Microvision Inc. (HMI) electron beam mask inspection tool with a sensitivity of <20 nm. Sematech has also demonstrated short run imprint defectivity of only 0.09/cm^2 as measured by a KLA-T 2800 wafer-inspection tool with sensitivity on the order of 30 nm.[10] Toshiba is now evaluating electrical test results of imprinted wafers and has demonstrated yield of short (0.75 mm) testers at a half pitch of 24 nm. In addition, half pitches of 26 and 32 nm have yielded for lengths exceeding 1 and 10 m, respectively.[11]

Excellent progress on mask defectivity makes it possible to easily separate defects generated from the mask and from the imprint process. Defects occurring during imprinting can generally be broken into two categories: random defects and repeating defects. Examples of random defects include plug defects, line collapse, and nonfill defects. Examples of repeater defects include mask defects and particle-induced defects. Previous studies have indicated that soft particles tend to cause nonrepeating defects. Hard particles, on the other hand, can cause either permanent resist plugging or mask damage. This work summarizes the results of defect inspections focusing on two key defect types: random nonfill defects occurring during the resist filling process and repeater defects caused by interactions with particles on the substrate.

Nonfill defectivity must always be considered within the context of process throughput. Processing steps such as resist exposure time and mask/wafer separation are well understood, and typical times for the steps are on the order of 0.10–0.20 s. To achieve a total process throughput of 20 wafers per hour (wph), it is necessary to complete the fluid fill step in 1.0 s, making it the key limiting step in an imprint process. As a result, it is critical to characterize the filling process by measuring nonfill defectivity as a function of fill time. In this work, an Imprio 500 20-wph development

1932-5150/2011/$25.00 © 2011 SPIE

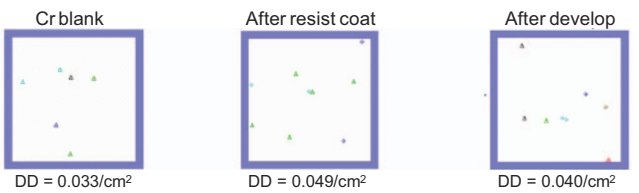

Fig. 1 Defect density on a mask blank after chromium deposition, after resist coat, and after resist develop.

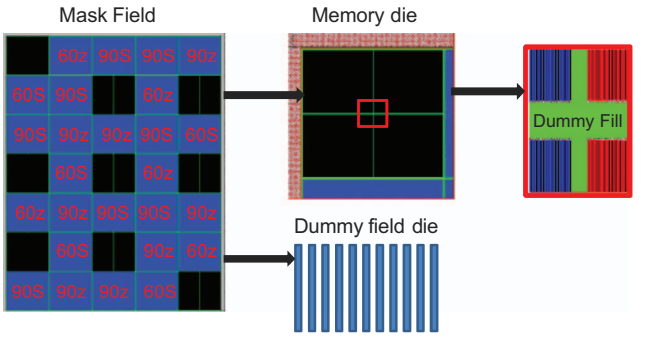

Fig. 2 Mask layout used for studying nonfill defects.

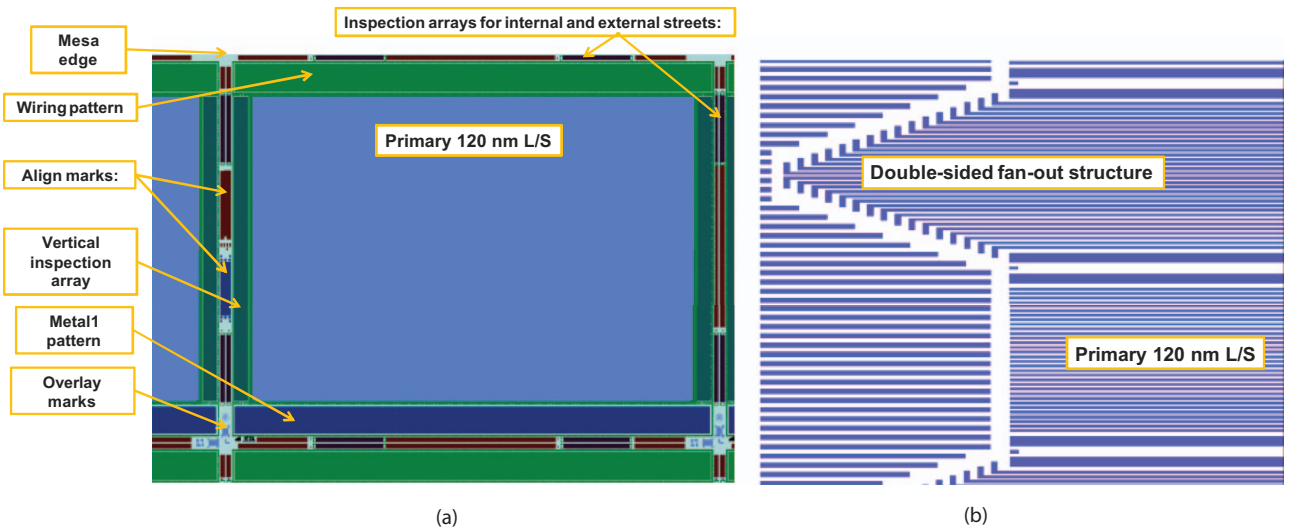

Fig. 3 (a) Repeating die including the 120-nm primary pattern and (b) magnified view of the primary pattern.

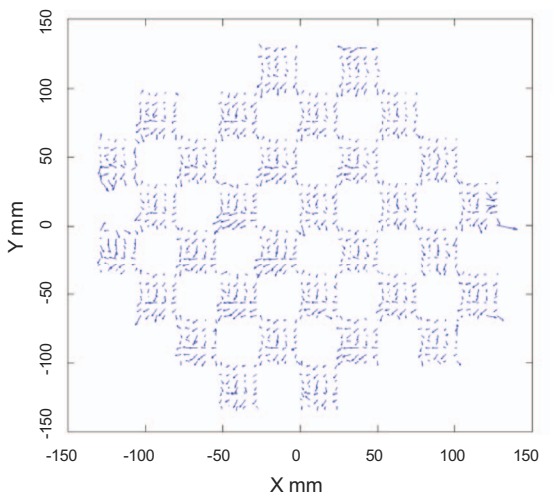

Number of fields measured: 32
Number of points per field: 30

	X	Y
Raw Mean	-0.10	-0.63
Raw 3sigma	9.40	9.68
Mean + 3sigma	**9.5**	**10.31**

Fig. 4 Mix-and-match overlay using an Imprio 500 development tool.

tool was used to study nonfill defectivity. By carefully controlling the volume of inkjetted resist, optimizing the drop pattern, and controlling the resist fluid front during spreading, throughputs of close to 1.5 s were achieved with nonfill defect levels of ~1.2/cm^2.

In a previous study, particles were shown to cause either repeating resist plugging or, in a limited number of cases, mask damage.[12] An Imprio 300, a 4-wph wafer per hour technology demonstrator tool, was used to identify sources of particle defects. This particular tool is set up to run 200-mm wafers, thereby allowing full wafer inspection. Longevity runs were used to study repeater defects, and a nickel contamination was identified as the key source of particle-induced repeater defects.

2 Experimental Details

2.1 *Imprint Process*

To generate the inspection test masks, patterns were exposed by Dai Nippon Printing using a NuFlare EBM7000 shaped beam pattern generator. ZEP520A resist was chosen as the positive imaging resist. After development, the chromium and fused silica were etched using Cl_2/O_2 and fluorine-based chemistry, respectively. Mesa lithography and a mesa etch process were employed to create a finished imprint mask for the Imprio 500 tool. For the Imprio 300, an additional dice-and-polish step was required to create the final mask.[13]

The pattern chosen for evaluation of nonfill defects was a 26 × 33 mm mask consisting of 28-nm flashlike devicelike gate patterns and dummy fill die surrounding the device die. The mask also included peripheral structures, such as align marks and metrology marks. A schematic of the mask layout is shown in Fig. 2.

A second 26 × 33 mm mask was used to study repeater defects. A primary die, consisting of 120-nm NAND flashlike features surrounded by additional metrology, alignment, and test cells, was designed to simulate a standard memory gate layer. The die breakdown along with a close up of the primary pattern is shown in Figs. 3(a) and 3(b). The primary pattern was sized for compatibility with in-house inspection sensitivity.

Imprinting of the 120-nm mask pattern was performed by using a Molecular Imprints Imprio® 300 imprint tool. A drop-on-demand method was employed to dispense the photopolymerizable acrylate-based imprint solution in field locations across a 200-mm silicon wafer. The template was then lowered into liquid contact with the substrate, displacing the solution and filling the imprint field. UV irradiation through the back side of the template cured the acrylate monomer. The process was then repeated to completely populate the substrate. Details of the imprint process have previously been reported.[8,14,15] The 28-nm mask was printed on an Imprio 500 development tool. Both wafer throughput and overlay are improved on this system relative to the Imprio 300. Throughput and mix-and-match overlay are specified at 20 wph and 15 nm, 3σ, respectively. An example of a 10-nm overlay, using a previous baseline fill time of 8 s, is shown in Fig. 4.

2.2 *Inspection Details*

An in-house KLA-Tencor 2132 200-mm wafer inspection tool, with sensitivity on the order of 100 nm, was used to examine the printed fields. Particle defects are readily detected, even at a relaxed sensitivity. In order to understand whether the sensitivity of the KLA-T 2132 was sufficient to study nonfill defects, a test was run with the 120-nm mask. A baseline imprint recipe was run, with filling times of 6 and 8 s. Nonfill defects were then counted using both a KLA-T 2132 and a more sensitive KLA-T 2800 wafer inspection system. Defect counts were then compared for each tool. At 6 s, the nonfill defect density for the 2132 and 2800 was 3.5/cm^2 and 6.9/cm^2. At 8 s, the defect density was reduced to 1.2/cm^2 and 1.7/cm^2. The 6-s results are shown in Fig. 5. Note that the defect locations are nearly identical for each defect map, indicating that although the 2800 has superior resolution capability, the 2132 tool is sufficient for understanding fluid filling and evaluating nonfill defect trends.

3 Defect Results

3.1 *Nonfill Defects*

Fluid resist fill time is influenced by several factors. Drop volume plays a critical role. By using smaller drop volumes, individual drops can be placed closer together, thereby minimizing the volume of trapped gas between each drop. Fluid front control is also a key contributor. Careful shaping of the mask surface as it makes contact with the imprint fluid also reduces trapped gas and improves filling time. Finally, the drop pattern used to fill the mask relief features affects fill time by minimizing the liquid travel. Careful consideration of the patterned features also plays a role. As an example, it is readily observed that filling is accelerated along the length of parallel lines, such as one finds in a flash gate layout. An initial attempt at accelerating fill time through the use of tailored dummy patterns has been introduced into the 28-nm mask layout described in Sec. 2.1. Further refinement of imprint specific dummy patterns [design for imprint (DFI)] will be the subject of future papers.

A series of three experiments were performed on the Imprio 500 in an attempt to reduce fluid fill time. In the first experiment (see Fig. 5), nonfill defect density was measured as a function of drop volume. Drop volumes were set to 2.8, 3.1, and 3.5 pL. The shaded boxes indicate the use of a standard 8-s fill time. The white boxes used a reduced fill time of 3 s. A point within the field indicates a location where a nonfill defect was detected. Nonfill defectivity clearly decreases as a function of reduced drop volume. The chart on the right-hand side of Fig. 6 depicts a drop in defect density of nearly an order of magnitude simply by reducing the drop volume from 3.5 to 2.8 pL.

In the second test, fluid front control was optimized by adjusting the spread-time velocity such that a more constant velocity was achieved across the printed field. Drop volume

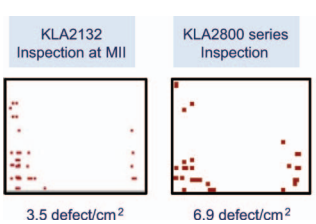

	8sec fill Defectivity [defect/cm^2]	6sec fill Defectivity [defect/cm^2]
KLA-T 2132	1.2	3.5
KLA-T 2800	1.7	6.9

Fig. 5 Nonfill defect density after a 6-s fill time as measured using KLA-T 2132 and KLA-T 2800 wafer inspection systems. Defect densities and defect locations are comparable for each tool.

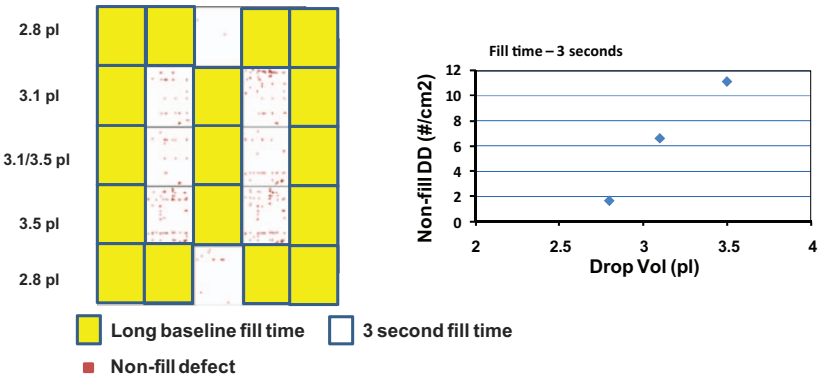

Fig. 6 Field defect maps as a function of fill time and drop volume. An order of magnitude reduction is realized by decreasing resist drop volume from 3.5 to 2.8 pL.

was held constant at 2.8 pL. The results are shown in Fig. 7. A fill time of 2.5 s with a nonfill defect density of zero was achieved. Although the defectivity jumps to 3.6/cm^2 at 2 s, it should be noted that the defects always occur at one edge of the mask field, suggesting that the defects are systematic and can be eliminated with further optimization of either the system controls or the drop pattern.

In the final test, further optimization of the drop pattern was achieved by using gridded patterns in areas where the features were essentially parallel lines. In addition, the drop volume was further decreased to 1.5 pL. The results are shown in Fig. 8. Figure 8(a) depicts the location of each defect within the printed mask field for a fill time of 1.5 s. Although the defectivity (1.2/cm^2) is higher than the targeted value of 1.0/cm^2, it should be noted that the defects are again systematic. Two types of nonfill defects are observed. The first are the nonfill defects within the printed Moiré align mark [see Fig. 8(b)]. The second defect always occurs in transition areas between a repeating structure in a die and another pattern type. Both defects can likely be addressed with specific imprint patterns designed to enhance filling in these areas.

3.2 *Repeater Defect Analysis*

Previous printing studies have identified two primary sources of repeater defects: defects originating on the mask and defects generated by particles on the wafer or mask surface. Because the mask touches the liquid resist during the fill process, extra care must be taken in preparing wafers for imprinting. Precautions include the use of low-defect silicon wafers and aggressive filtration of both the adhesion layer and imprint fluid. Assuming this is addressed, the main source of repeater defectivity can be attributed to particles generated by the imprint tool itself. Careful wafer cycling tests indicate that particle adders in the tool can be as low as 0.1 per wafer pass. To determine the root cause of the particles, the 120-nm mask described in Sec. 2(a) was used to track defectivity. To eliminate wafer-related particles, only fields that were confirmed to have particles of <70 nm (as measured using a KLA-T SP1 blank wafer inspection system) were printed. The wafers were then inspected using the KLA-T 2132, and the repeater defect locations were identified. Composition of the defect was then determined by placing the wafer in a scanning electron microscope (SEM), driving to the location where the repeater defect was first reported and performing an EDX measurement at the defect site.

All but one of the defects were confirmed to contain nickel. Figure 9 shows both a picture of the particle and the EDX measurements. Figure 9(a) shows the EDX signal within the defective area. Figure 9(b) is a scan of a clean pattern. The nickel peak is clearly observed, and every defect containing nickel showed a comparable signal intensity. It should be noted that both the inkjet dispenser and the filter unit contained within the imprint tool both contain nickel parts. We are currently investigating the dispense-and-filter design and are planning future work to either eliminate or filter out this potential source of contamination.

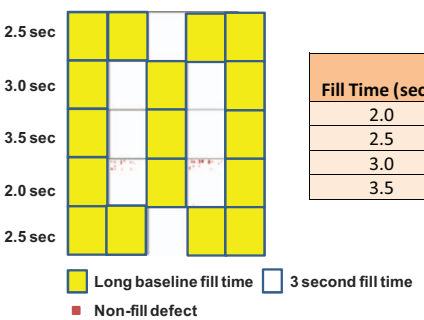

Fill Time (secs)	Defect Density (cm^{-2})
2.0	3.6
2.5	0
3.0	0
3.5	0

Fig. 7 Nonfill defectivity after optimizing the fluid front control. Fill times of 2.5 s are achieved with no defects.

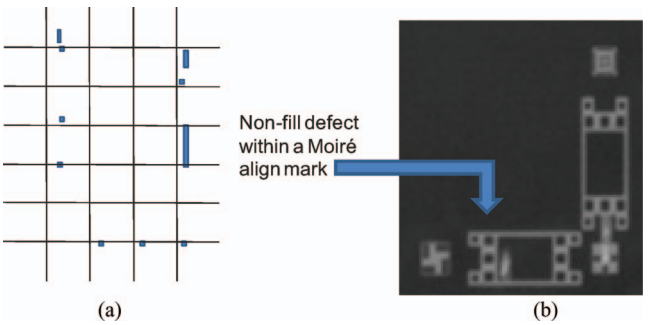

Fig. 8 (a) Field defect map showing the locations of nonfill defects using a fill time of 1.5 s and (b) An example of a nonfill defect within a printed Moiré align mark.

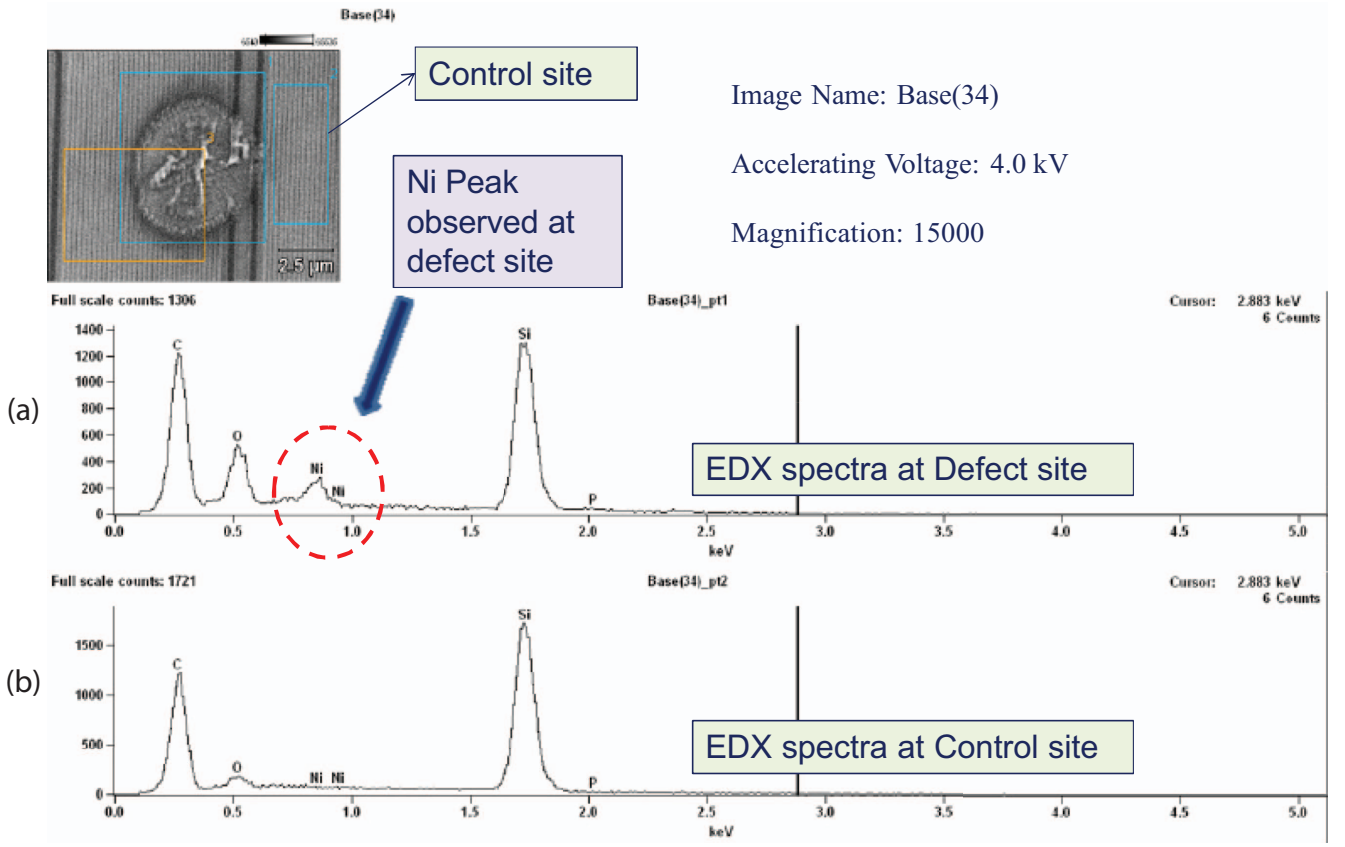

Fig. 9 (a) EDX of the particle causing a repeater defect and (b) EDX of a cleanly printed adjacent site.

4 Conclusions

Excellent progress continues to be made on reducing defectivity. A mask blank defectivty of 0.04/cm^2 has been demonstrated and patterned mask defectivity has been reduced to 10/cm^2 (without mask repair). Imprint defects have been classified, and overall short-run defectivity has been reduced by making improvements to the resist, tool, and imprint process. Sematech has achieved imprint defectivity of <0.10/cm^2, and the process has improved to the point where electrical test structures are now yielding at half pitches as small as 24 nm.

Nonfill defect densities of 1.2/cm^2 are now being obtained for fill times of 1.5 s. In order to hit the throughput target of 20 wph, it will be necessary to cut fill times to 1.0 s and perform overlay in parallel with the filling process. It is anticipated that smaller drop volumes, improved drop patterns, and pattern design for imprint will allow this reduction in fill time.

The overall program goal for defectivity is to print 50,000 fields at defect densities of <1.0/cm^2. Although this goal is not as aggressive as the International Technology Roadmap for Semiconductors (ITRS) defect specification, it should be noted that the insertion of imprint lithography is targeted at nonvolatile memory, where redundancy permits a more relaxed defectivity specification. The key to meeting this goal is the identification and elimination of particles that interfere with the imprint process. A nickel-based contaminant has been identified, and work is underway to verify the source of the nickel. It should also be noted that recent improvements to the formation of the align marks have addressed mark contamination issues, and future experiments will need to confirm low defectivity for extended imprint runs.[9] The final step in defect control is the placement of high-end tools at customer sites. Future work will exercise both an Imprio 500 tool and a customized imprint module (Molecular Imprints) in preparation for production readiness.

Acknowledgments

The authors thank Masaaki Kurihara, Shiho Sasaki, Koji Ichimura, and Naoya Hayashi, from Dai Nippon Printing, for their excellent imprint mask fabrication work. The authors are also grateful to Masayuki Hatano and Takuya Kono, from Toshiba, and Matt Malloy and Lloyd Litt, from Sematech, for sharing their imprint results.

References

1. S. Y. Chou, P. R. Kraus, and P. J. Renstrom, "Nanoimprint lithography," *J. Vac. Sci. Technol. B* **14**(6), 4129–4133 (1996).
2. T. K. Widden, D. K. Ferry, M. N. Kozicki, E. Kim, A. Kumar, J. Wilbur, and G. M. Whitesides, "Pattern transfer to silicon by microcontact printing and RIE," *Nanotechnology* **7**, 447–451 (1996).
3. M. Colburn, S. Johnson, M. Stewart, S. Damle, T. Bailey, B. Choi, M. Wedlake, T. Michaelson, S. V. Sreenivasan, J. Ekerdt, and C. G. Willson, "Step and flash imprint lithography: a new approach to high-resolution printing," *Proc. SPIE* **3576**, 379–389 (1999).
4. M. Colburn, T. Bailey, B. J. Choi, J. G. Ekerdt, and S. V. Sreenivasan, "Development and advantages of step-and-flash lithography," *Solid State Technol.* **44**(7), 67–76 (2001).
5. T. C. Bailey, D. J. Resnick, D. Mancini, K. J. Nordquist, W. J. Dauksher, E. Ainley, A. Talin, K. Gehoski, J. H. Baker, B. J. Choi, S. Johnson, M.

Colburn, S. V. Sreenivasan, J. G. Ekerdt, and C. G. Willson, "Template fabrication schemes for step and flash imprint lithography," *Microelectron. Eng.* **61–62**, 461–467 (2002).
6. F. Xu, M. Watts, V. Truskett, I. McMackin, J. Choi, P. Schumaker, E. Thompson, D. Babbs, S. V. Sreenivasan, and N. Schumaker, "Development of imprint materials for the Step and Flash Imprint Lithography process," *Proc. SPIE* **5374**, 232–241 (2004).
7. K. Selenidis, J. Maltabes, I. McMackin, J. Perez, W. Martin, D. J. Resnick, and S. V. Sreenivasan, "Defect reduction progress in step and flash imprint lithography," *Proc. SPIE* **6730**, 67300F (2007).
8. I. McMackin, J. Choi, P. Schumaker, V. Nguyen, F. Xu, E. Thompson, D. Babbs, S. V. Sreenivasan, M. Watts, and N. Schumaker, "Step and repeat UV nanoimprint lithography tools and processes," *Proc. SPIE* **5374**, 222–231 (2004).
9. K. S. Selinidis, C. B. Brooks, G. F. Doyle, L. Brown, C. Jones, J. Imhof, D. L. LaBrake, D. J. Resnick, and S. V. Sreenivasan, "Progress in mask replication using jet and flash imprint lithography," *Proc. SPIE* **7970**, 797009 (2011).
10. M. Malloy and L. Litt, "Jet and flash imprint defectivity: assessment and reduction for semiconductor applications," *Proc. SPIE* **7970**, 797006 (2011).
11. T. Higashiki, T. Nakasugi, and I. Yoneda, "Nanoimprint lithography for semiconductor devices and future patterning innovation," *Proc. SPIE* **7970**, 797003 (2011).
12. D. J. Resnick, G. Haase, L. Singh, D. Curran, G. M. Schmid, K. Luo, C. Brooks, K. Selinidis, J. Fretwell, and S. V. Sreenivasan, "Inspection of imprint lithography patterns for semiconductor and patterned media," *Proc. SPIE* **7637**, 76370R (2010).
13. L. Jeff Myron, L. Gershtein, G. Gottlieb, B. Burkhardt, A. Griffiths, D. Mellenthin, K. Rentzsch, S. MacDonald, and G. Hughes, "Advanced mask metrology enabling characterization of imprint lithography templates," *Proc. SPIE* **5752**, 384–391 (2005).
14. J. Choi, K. Nordquist, A. Cherala, L. Casoose, K. Gehoski, W. J. Dauksher, S. V. Sreenivasan, and D. J. Resnick, "Distortion and overlay performance of UV step and repeat imprint lithography," *Microelectron. Eng.* **78–79**, 633–640 (2001).
15. J. Perez, K. Selinidis, S. Johnson, B. Fletcher, F. Xu, J. Maltabes, I. McMackin, D. Resnick, and S. V. Sreenivasan, "A study of imprint-specific defects in the step and flash imprint lithography process," *Proc. SPIE* **6517**, 65170L (2007).

Biographies and photographs of the authors not available.